Proceedings of the Thirty-fourth (2024) International Ocean and Polar Engineering Conference **www.isope.org**
Rhodes, Greece, June 16–21, 2024

ISBN 978-1-880653-78-4; ISSN 1098-6189

Numerical Study of Liquid Sloshing in Partially Filled Spherical Tanks under Different Excitation Parameters

Chengjiang Xiao[1], Jifei Wang[2], Weiwen Zhao[1], Decheng Wan[1]*

[1] Computational Marine Hydrodynamic Lab (CMHL), School of Naval Architecture, Ocean and Civil Engineering, Shanghai Jiao Tong University, Shanghai, China
[2] Shanghai Aerospace System Engineering Institute, Shanghai, China

[*]Corresponding author

ABSTRACT

Under the influence of external excitations, liquid in tank will generate fluctuation, which is known as liquid sloshing. Due to its complexity and potential disturbance for the tank, many scholars have devoted to the study of liquid sloshing. In this paper, the liquid sloshing of spherical tank with different filling ratios and excitation parameters are numerically investigated. The free surface is solved with an artificially compressed volume of fluid (VOF) method. The excitation is achieved by a dynamic mesh motion which uses a prescribed motion on the liquid tank hull boundary. Free decay simulations are performed for two different liquid filling ratios. Natural frequency and damping ratio are extracted from the decay time histories of the liquid mass center. In addition, sloshing under sinusoidal excitations have been simulated under different excitation amplitudes and frequencies. The sloshing forces are analyzed and the relationship between sloshing force frequency and filling rate, as well as excitation frequency are discussed. Further, the free surface flow field under different case conditions are presented and analyzed. Parametric resonances are observed under some certain conditions.

KEY WORDS: liquid sloshing; spherical tank; OpenFOAM; parametric resonance

INTRODUCTION

Sloshing phenomena occur in various engineering flows, including the movement of fluids in storage systems like liquid cargo ships (e.g. LNG, LPG, and crude oil tankers) during navigation, rocket liquid fuel tanks during flight, nuclear reactors during earthquakes, and reservoirs. Sloshing can cause harm and must be prevented. For instance, during spaceflight, the agitated liquid can exert significant pressure on the fuel bulkhead of the satellite, resulting in deformation and damage to the structure. Similarly, the sloshing of the liquid in the fuel storage tank can disrupt the vehicle's control system, and it is possible to force the aircraft to deviate from the control orbit, or even lose stability and crash. Therefore, the study of liquid sloshing characteristics is an extremely important topic for engineering problems. Although liquid sloshing can have adverse effects, it is widely utilized as a passive damping mechanism in various engineering applications, including floating offshore wind turbines (Zhou et al., 2023) and high-rise building system (Das et al., 2020).

Liquid sloshing in tanks have been studied in the past decades. In a recent paper, Zheng et al. (2021) reviewed the study of liquid sloshing and pointed out that an increasing number of researchers have studied liquid tank sloshing and motivated a lots of theoretical, experimental and numerical studies. Theoretical and experimental method are the main method in earlier study. An experimental investigation of liquid sloshing in spherical and oblate-spheroidal tank was conducted by Sumner (1965) to determine the general characteristics. Aslam et al. (1979) conducted experiments in annular tanks to study the earthquake induced sloshing of water. To quantify the influence of sloshing aircraft fuel on wing vibrations, Martinez-Carrascal and González-Gutiérrez (2021) analyzed the effects of sloshing based on vertical single degree of freedom (DOF) sloshing tank experiments. While it can set complex sloshing situation and has the specific phenomenon, it requires much time and economic costs.

Some researchers use equivalent mechanical model (EMM) to predict sloshing forces for its efficiency. EMM such as pendulum or spring-mass or mix system was developed for approximate simulation of the characteristic of liquid sloshing. Sumner (1965) used pendulum analogy parameters to couple with the stabilization-control frequency or the fundamental body-bending frequency of the liquid tank. Zheng et al. (2012) proposed a method based on trammel pendulum's sloshing to obtain the distribution of sloshing force and torque during the sloshing process of a liquid tank. Perez et al. (2012) described the shaking dynamics of propellant storage tanks and determine model parameters by analyzing and testing different discrete filling levels. Sun et al. (2019) proposed a spring-mass model to analysis a rigid cylindrical tank with annular baffle. However, due to the simplification of EMMs, many

factors in sloshing were omitted. It is difficult to improve the accuracy and provide further insights from detailed flow field.

With the development of computer technology and computational fluid method (CFD), numerical method is becoming more and more popular. Godderidge et al. (2009) numerically investigated different approaches of the lateral sloshing rectangular tank and compared with experimental data. The simulation of the inhomogeneous multiphase model gives good agreement with the experimental pressure data. Yang et al. (2012) concluded that the CFD tool can accurately predict the sloshing natural frequency and low damping ratio of free decay by simulating different filling ratio and different sizes of smooth wall cylinder tank, which further validates the CFD technology in modelling the sloshing dynamics of space vehicle propellants. Further investigation of the sloshing was studied. Lu et al. (2015) simulated the model of two-dimensional viscous liquid sloshing in a rectangular tank with/without baffles and compare it with potential flow solutions. They found that with power-law excitation, the relative sloshing amplitudes decrease around the resonance condition, and addresses the need for the viscous model in sloshing prediction. Yu et al. (2017) studied the sloshing of a rectangular liquid tank with two floating plates in experimental and numerical studies to investigate the performance of the suppression device and the corresponding mechanisms. Das et al. (2020) study the U-shaped containers sloshing in experimental and numerical method to test its efficacy as liquid dampers in high-rise building system. Zhang et al. (2022) to simulate and analysis the Faraday wave in heave excited sloshing tank by improved MPS method.

The objective of the present study is to investigate the liquid sloshing for partially filled spherical tanks under different conditions. The paper first introduces the numerical method, then the geometry, case condition and numerical discretization is presented. Followed by the discussion and analyzation of sloshing forces and free surface flow fields. Finally the conclusion is drawn.

NUMERICAL METHOD

All the numerical simulations are performed with the computational fluid dynamics (CFD) solver naoe-FOAM-SJTU (Wang et al., 2019), which is a two-phase incompressible flow solver based on OpenFOAM.

Governing equation

In this study, flow conditions are assumed to be laminar. The fluid for tank sloshing is a two-phase unsteady incompressible viscous fluid, and its governing equations can be written as:

$$\nabla \cdot \mathbf{U} = 0 \tag{1}$$

$$\frac{\partial \rho \mathbf{U}}{\partial t} + \nabla \cdot (\rho \mathbf{U}\mathbf{U}) = -\nabla p_d - \mathbf{g} \cdot \mathbf{x} \nabla \rho + \nabla \cdot \left(\mu \nabla \mathbf{U}\right) + f_\sigma \tag{2}$$

where, ρ is the fluid density, $\mathbf{U}$ is the velocity vector, $p_d = p - \rho \mathbf{g} \cdot \mathbf{x}$ presents the dynamic pressure, μ is the kinematic viscosity, $\mathbf{g}$ is gravitational acceleration vector, t indicates the time. f_σ is the surface tension force.

Free surface capturing

To capture the free surface, the Volume of Fluid (VOF) method with artificial compression term is utilized (Berberović et al., 2009). The advantage of this artificial interfacial compression technique is that it can control numerical dissipation and has high accuracy in capturing free surfaces. The VOF method solves a transport equation in terms of volume fraction of fluid. The transport equation can be defined as:

$$\frac{\partial \alpha}{\partial t} + \nabla \cdot (\mathbf{U}\alpha) + \nabla \cdot \left[\mathbf{U}_r \alpha (1-\alpha)\right] = 0 \tag{3}$$

where, $\mathbf{U}_r = \mathbf{U}_l - \mathbf{U}_g$ is the relative velocity, defined as compression velocity. The subscripts g and l represent gas and liquid respectively. α is the volume fraction and represents the relative percentage of the fluid in each cell grid :

$$\begin{cases} \alpha = 0 & \text{air} \\ \alpha = 1 & \text{water} \\ 0 < \alpha < 1 & \text{freesurface} \end{cases} \tag{4}$$

Based on the volume fraction α , density ρ and dynamic viscosity μ can be defined as:

$$\begin{cases} \rho = \alpha \rho_l + (1-\alpha)\rho_g \\ \mu = \alpha \mu_l + (1-\alpha)\mu_g \end{cases} \tag{5}$$

Dynamic mesh

In this paper, the dynamic mesh is utilized to simulate the external excitation of the spherical liquid tank. All the grid points are moved along with a prescribed sinusoidal displacement boundary on the wall surface, whose grid points displacement can be written as follows:

$$x = x_0 \sin(\omega_e t) \tag{6}$$

where, x represents the displacement on x-axis, x_0 represents the amplitude of displacement excitation, ω_e represents circular frequency of displacement excitation.

Free decay parameters extraction

In order to obtain natural frequency and damping ratio of liquid tank at different filling rates, free decay simulations are carried our firstly and record the center of gravity(COG) in time history. Generally, the figure will be shown like Fig. 4. From the statistics, natural frequency is easy to calculate by time intervals between different wave peaks or troughs. Considering average, the natural frequency can be expressed as:

$$\omega_0 = \frac{2\pi n}{(T_{i+n} - T_i)} \tag{7}$$

where, T_i and T_{i+n} represent the time corresponding to the (i)-th and (i+n)-th wave peak, respectively; and n represents the number of intervals between two wave peaks.

The damping ratio for free decay in accordance with the logarithmic decay rate is expressed as:

$$\gamma = \frac{1}{2\pi n} \ln\left(\frac{A_i}{A_{i+n}}\right) \tag{8}$$

where, A_i and A_{i+n} represent the amplitude corresponding to the (i)-th and (i+n)-th wave peak, respectively.

The natural frequency of the free decay can be obtained by averaging the time intervals between different wave peaks or troughs. Through the above free-decaying centre-of-mass motion time-example curve, the natural frequency and damping of free decay can be extracted according to the above calculation method.

NUMERICAL SIMULATIONS

Geometry and case conditions

The sketch of geometry model is shown in Fig. 1. The spherical tank set in the work has the radius of R=0.25m, and the liquid height above the bottom of the tank is h. A partially filled spherical liquid tank sloshes under horizontal sinusoidal excitation, with an excitation amplitude of x_0 . the excitation frequency is ω_e , and the natural frequency of the tank is ω_0 .

Two different filling rates of h/R=0.4 and 1.6 are selected for calculation, with non-dimensional frequency ω_e / ω_0 =0.4,0.6,0.8 and 1 and non-dimensional amplitude x_0/R=0.005,0.01,0.03 and 0.06. A series of cases with different excitation parameters are listed in Table 1.

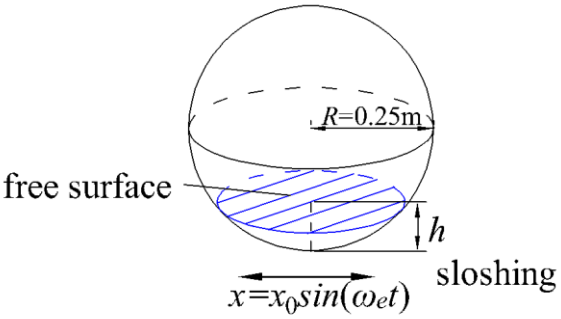

Fig. 1 The sketch of 3-D spherical tank.

Computational mesh and boundary condition

Fig. 2. shows the mesh on a cross-section of the liquid tank sphere. The computational mesh has a uniform cell size of 0.02R. The total number of mesh is 380 thousand. The boundary condition of velocity is zero normal gradient, and for pressure the boundary condition is set to *fixedFluxPressure*, which sets the pressure gradient so that the flux on the boundary is that specified by the velocity boundary condition.

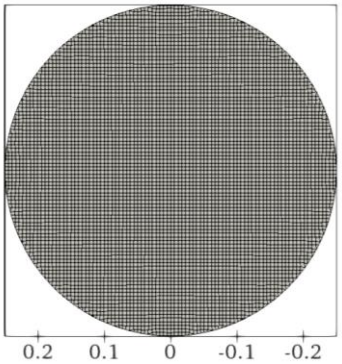

Fig. 2 Computational mesh

Two numerical cases of free decay were used in order to get the ω_0 of two different filling rates, and 20 cases with concrete external excitation condition are shown in Table. 1.

Cases 1-4 and 11-14 are closer to the actual parameter performance when the liquid tank is affected by sloshing under normal operating conditions, and the purpose of the supplementary examples is to explore the more general sloshing laws of spherical liquid tanks.

Table. 1 The case with different sloshing condition.

Case	h/R	ω_e / ω_0	x_0/R	Notes
1	0.4	0.4	0.005	Low filling rate and slight sloshing
2			0.01	
3		0.6	0.005	
4			0.01	
5			0.03	Low filling rate and significant sloshing
6			0.06	
7		0.8	0.03	
8			0.06	
9		1	0.03	
10			0.06	
11	1.6	0.4	0.005	High filling rate and slight sloshing
12			0.01	
13		0.6	0.005	
14			0.01	
15			0.03	High filling rate and significant sloshing
16			0.06	
17		0.8	0.03	
18			0.06	
19		1	0.03	
20			0.06	

Numerical discretization

In this paper, the second-order backward scheme is adopted to discretized the temporal term. For spatial discretization, the convection term is discretized with *Gauss linearUpwind limitedGrad* scheme. The Laplacian term is discretized with *Gauss linear corrected* scheme. The coupled pressure and velocity term is solved by PIMPLE algorithm, which is a merged PISO-SIMPLE method. The solving steps of the PISO method are firstly estimated by one step and then correct two steps. The PIMPLE method differs from the original PISO method in which it performs several cyclic corrections within the same time step. The last correction result is taken as the initial value for the next time step, and the above iteration is continued.

Mesh convergence validation

To validate the result, a series of numerical tests were conducted for Case 7 using meshes of varying refinement. Table. 2 presents the total number of elements for each mesh configuration along with the maximum sloshing force on the x-axis observed during the interval 55-60 seconds (approximately at 57.4 seconds). Fig. 3 illustrates the time history of the sloshing force for these three tests, indicating that the curves are nearly identical. Notably, the performance of the medium refinement mesh closely approximates that of the finest mesh, with force values showing

negligible variation (a relative error of less than 2%). These results suggest that the mesh has achieved convergence, and employing a medium refinement mesh strikes an optimal balance between computational efficiency and accuracy.

Table. 2 Mesh convergence test for case7.

Mesh	Total number	Maximum Sloshing force(N)
Coarse	267608	4.507
Medium	380724	4.620
Fine	522448	4.708

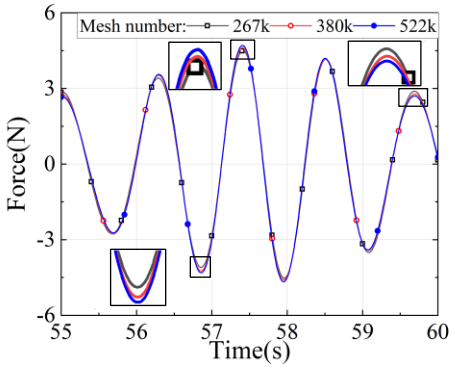

Fig. 3 Time history of sloshing force for mesh refinement test

RESULTS AND DISCUSSIONS

Free decay analysis

The numerical simulation of free decay is carried out using a preset initial inclination angle of the liquid surface. The initial inclination angle of the liquid surface is set to 5 deg, and then numerical simulation is carried out. The liquid motion will freely decay due to the gravity. The time history of the center of gravity in *x*-axis of two different filling ratios is shown in Fig. 4 and the extracted natural frequency and damping ratio are listed in Table 3. It can be seen that when the filling rate is high, the natural frequency and damping ratio is increasing. This is mainly because the mass involved in sloshing increases.

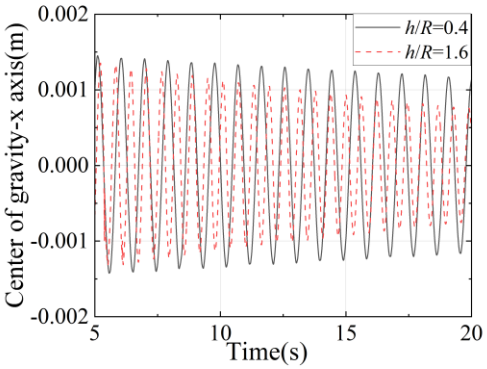

Fig. 4 Time history of center of gravity in x-axis

Table. 3 The extracted natural frequency and damping ratio

h/R	Natural frequency(rad/s)	Damping ratio
0.4	6.74	0.00219
1.6	10.27	0.00376

Effect of different excitation amplitudes

In order to study the influence of the excitation amplitudes under low liquid filling rate, a series of amplitude and frequency ratio, corresponding cases 1-10.

Fig. 5 shows the time history and Fast Fourier transform (FFT) analysis of small-amplitude sloshing under low filling rate conditions in cases 3-6. By analyzing the sinusoidal excitation with a liquid filling rate of 0.4, a non-dimensional frequency of 0.6, and a series of non-dimensional excitation amplitudes x_0/R=0.05, 0.01, 0.03, and 0.06, the maximum of sloshing force in the same change period in 60-65s is 0.244, 0.608, 1.913, 3.908N respectively. Through the FFT analysis, two main frequencies appear in sloshing force, which are excitation frequency and natural frequency respectively, and the energy at the excitation frequency is greater than the energy at the natural frequency.

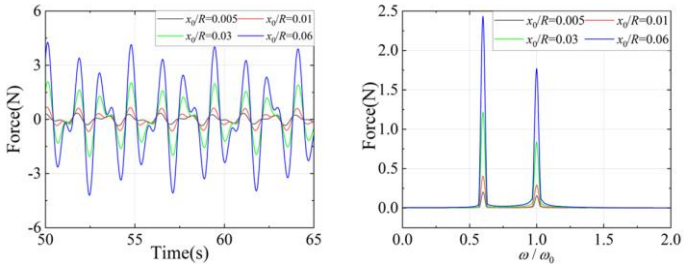

Fig. 5 Time history and FFT of x-direction sloshing force in cases 3-6, h/R=0.4, ω_e / ω_0 =0.6, x_0/R=0.005,0.01,0.03,0.06.

Effect of different excitation frequency

Fig. 6 and Fig. 7 display a series of sloshing condition with different non-dimensional frequency and filling rate. From Fig. 6, it can be seen that with a nondimensional excitation frequency of 0.4 and filling rate of 0.4, the forces acting on the liquid tank are composed of sloshing of similar magnitude at the natural frequency and excitation frequency, and it can be found that as the liquid filling rate increases, the force amplitude of the contribution of natural frequency to sloshing force remains basically unchanged. While with the same filling rate and nondimensional frequency at 0.6 as shown in Fig. 5, the frequency of the excitation frequency affection to sloshing force is increasing.

Fig. 7 shows the sloshing force in time history and FFT of rest cases. When the ratio reaches 0.8, Fig. 7 (a)(c) shows that the sloshing force at high excitation frequencies is basically not affected under the same filling rate and excitation amplitude. Comparing Fig. 7 (b) with Fig. 7(d), the sloshing force at low filling rate is quite different with that at high filling rate. It is found that there are multiple frequencies for the low filling rate case, which will be further analyzed in next section.

Observing the sloshing force curve under high liquid filling rate, it can be seen that the curve has obvious periodic changes. This is mainly because the larger inertia force generated by forced vibration under high liquid filling rate, So although the excitation frequency is the same, the sloshing force of cases 19, 20 in Fig. 7(d) is quite different in comparison with case 9,10 in Fig. 7(b).

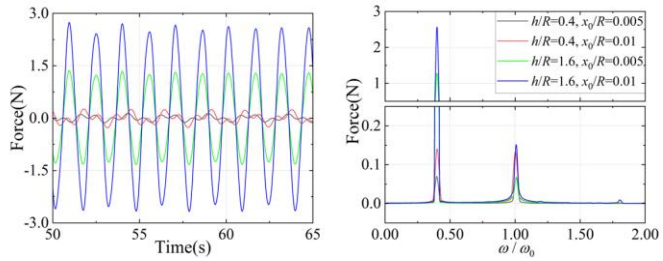

Fig. 6 Time history and FFT of x-direction sloshing force in cases 1,2,11,12. with h/R=0.4,1.6, ω_e / ω_0 =0.4, x_0/R=0.005,0.01

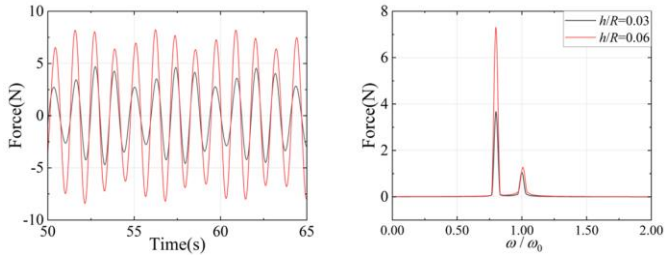

(a) cases 7,8. h/R=0.4, ω_e / ω_0 =0.8, x_0/R=0.03,0.06

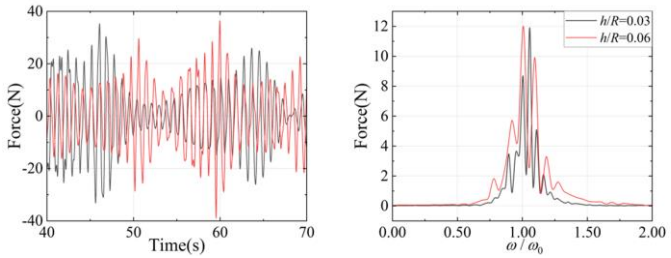

(b) cases 9,10. h/R=0.4, ω_e / ω_0 =1, x_0/R=0.03,0.06

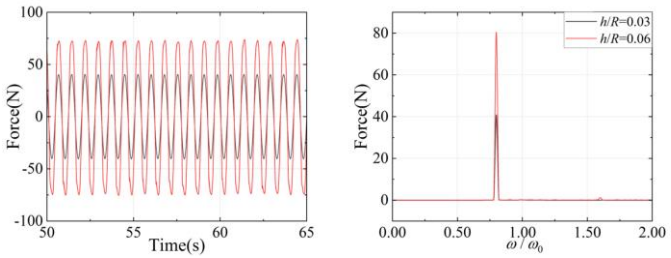

(c) cases 17,18. h/R=1.6, ω_e / ω_0 =0.8, x_0/R=0.03,0.06

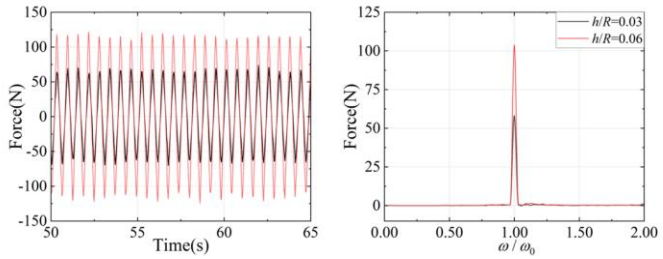

(d) cases 19,20. h/R=1.6, ω_e / ω_0 =1, x_0/R=0.03,0.06

Fig. 7 Time history and FFT of *x*-direction sloshing force.

Flow field analysis

Several cases are selected with obvious changes in free surfaces (cases 8-10, 17-20) for flow field analysis Fig. 6 shows the variation of the free surface flow field within one period in these cases.

From Fig. 8(a)(d)(e)(f), it can be seen that the flow field of case 18 with non-dimensional frequency of 0.8 shows the obvious non-linear phenomenon. The phenomenon of wave breaking appears in sloshing. While case 8 with lower filling rate, case 16 with lower excitation frequency and case 17 with lower excitation amplitude all show in stable linear flow field.

When the non-dimensional excitation frequency is further increased to ω_1 / ω_0 =1, corresponding to Fig. 7(b)(d), where the time history and FFT of sloshing force are presented. It can be observed that under the condition of low liquid filling rate, the fluid in the tank is rotating, as shown in Fig. 8(b)(c). This similar phenomenon was also observed in previous experimental and numerical studies (Xue et al., 2019). It is inferred that the main reason is that the liquid in the tank has a parametric resonance phenomenon during the sloshing process, which causes the motion of fluid to appear in another degree of freedom. While in high filling rates when resonance occurs, as shown in Fig. 8(h), the motion in the x direction of the flow field still plays a dominant role. The liquid in the tank itself has a large inertial force.

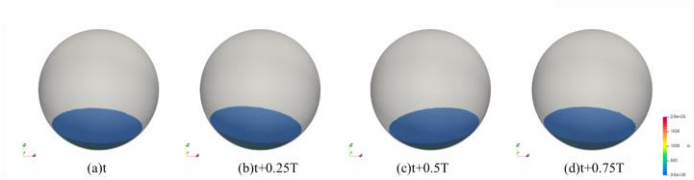

(a) case 8, h/R=0.4, ω_e / ω_0 =0.8, x_0/R=0.06

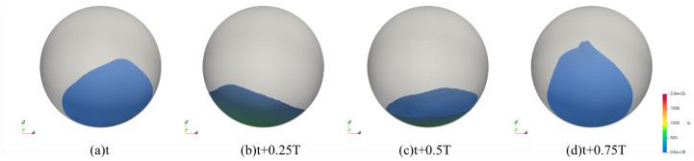

(b) case 9, h/R=0.4, ω_e / ω_0 =1, x_0/R=0.03

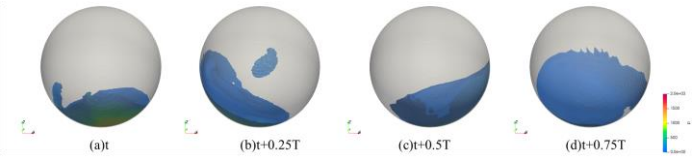

(c) case 10, h/R=0.4, ω_e / ω_0 =1, x_0/R=0.06

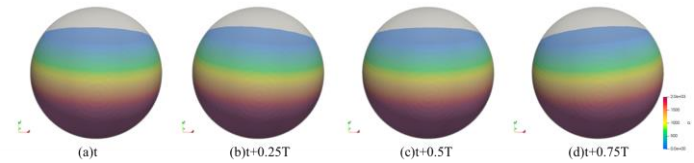

(d) case 16, h/R=1.6, ω_e / ω_0 =0.6, x_0/R=0.06

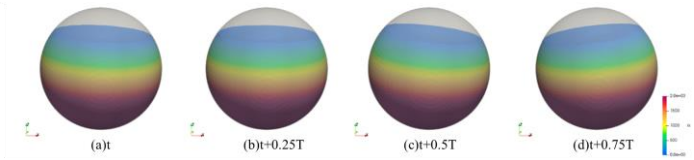

(e) case 17, h/R=1.6, ω_e / ω_0 =0.8, x_0/R=0.03

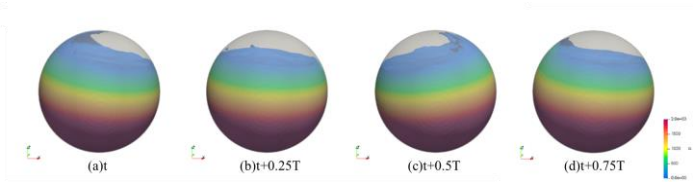

(f) case 18, h/R=1.6, ω_e / ω_0 =0.8, x_0/R=0.06

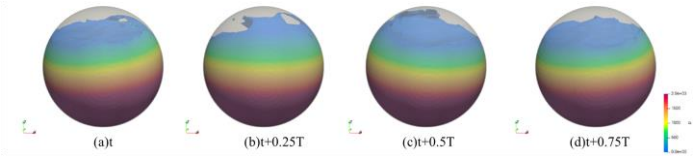

(g) case 19, h/R=1.6, ω_e / ω_0 =1, x_0/R=0.03

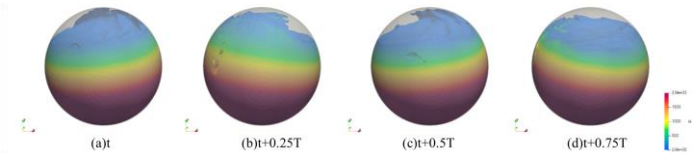

(h) case 20, h/R=1.6, ω_e / ω_0 =1, x_0/R=0.06

Fig. 8 Free surface flow field during one period

CONCLUSIONS

This paper uses the CFD solver naoe-FOAM-SJTU based on OpenFOAM to simulate and analyze the free decay experiments under two liquid filling rates to extract the natural frequencies and damping parameters. A series of numerical analysis are performed for the corresponding liquid filling rates of the model. The following conclusions are obtained:

1. As the filling rate increases, both the natural frequency and damping of the liquid tank increase. It can be inferred that in EMMs while the COG can be seen as a pendulum trajectory and the pivot of the pendulum is the center of spherical tank. As the filling rate increases, the pendulum length seen as length between COG and the center of the spherical tank is shorter, and the natural frequency is higher.

2. At low liquid filling rates, the frequency of sloshing force generated during sloshing is jointly affected by the excitation frequency and the natural frequency, and as the excitation frequency approaches the natural frequency, the sloshing force frequency is less affected by the natural frequency, and mainly affected by the excitation frequency. Under high liquid filling rates, it can be seen from the time history and FFT that the frequency of the sloshing force is basically consistent with the excitation frequency, and there is still energy distribution at the natural frequency. It can be seen from working conditions 5-8 that under the same liquid filling rate and forced vibration, the amplitude does not change the influence of the excitation frequency and the natural frequency on the tank.

3. When the excitation frequency is equal to the natural frequency, it is inferred that parametric resonance occurs especially in sloshing at low liquid filling rates. The flow field in the tank rotates, and the periodic distribution pattern of the sloshing force in the *x*-direction is no longer obvious and sloshing force in other directions appears. This phenomenon is agreed with the experiment. Under high liquid filling rate, the the *x*-direction sloshing force is still so regular is because the inertial force of the liquid is large.

ACKNOWLEDGMENTS

This work is supported by the National Natural Science Foundation of China (52131102), to which the authors are most grateful.

REFERENCES

Aslam, M, Scalise, DT, and Godden, WG (1979). "Earthquake Sloshing in Annular and Cylindrical Tanks," *J Eng Mech Div*, 105(3), 371–389.

Berberović, E, Van Hinsberg, NP, Jakirlić, S, Roisman, IV, and Tropea, C (2009). "Drop impact onto a liquid layer of finite thickness: Dynamics of the cavity evolution," *Phys Rev E*, 79(3), 036306.

Das, A, Maity, D, and Bhattacharyya, SK (2020). "Characterization of liquid sloshing in U-shaped containers as dampers in high-rise buildings," *Ocean Eng*, 210, 107462.

Godderidge, B, Turnock, S, Tan, M, and Earl, C (2009). "An investigation of multiphase CFD modelling of a lateral sloshing tank," *Comput Fluids*, 38(2), 183–193.

Lu, L, Jiang, S, Zhao, M, and Tang, G (2015). "Two-dimensional viscous numerical simulation of liquid sloshing in rectangular tank with/without baffles and comparison with potential flow solutions," *Ocean Eng*, 108, 662–677.

Martinez-Carrascal, J, and González-Gutiérrez, LM (2021). "Experimental study of the liquid damping effects on a SDOF vertical sloshing tank," *J Fluids Struct*, 100, 103172.

Perez, JG, Parks, R, and Lazor, DR (2012). "Validation of slosh model parameters and anti-slosh Baffle designs of propellant tanks by using lateral slosh testing," *28th Aerosp Test Semin*, Los Angeles, California.

Sumner, IE (1965). "Experimentally determined pendulum analogy of liquid sloshing in spherical and oblate-spheroidal tanks." NASA-TN-D-2737.

Sun, Y, Zhou, D, and Wang, J (2019). "An equivalent mechanical model for fluid sloshing in a rigid cylindrical tank equipped with a rigid annular baffle," *Appl Math Model*, 72, 569–587.

Wang, J, Zhao, W, and Wan, D (2019). "Development of naoe-FOAM-SJTU solver based on OpenFOAM for marine hydrodynamics," *J Hydrodyn*, 31(1), 1–20.

Xue, M-A, Chen, Y, Zheng, J, Qian, L, and Yuan, X (2019). "Fluid dynamics analysis of sloshing pressure distribution in storage vessels of different shapes," *Ocean Eng*, 192, 106582.

Yang, H, Purandare, R, Peugeot, J, and West, J (2012). "Prediction of Liquid Slosh Damping Using a High Resolution CFD Tool," *48th AIAAASMESAEASEE Jt Propuls Conf Amp Exhib*, Atlanta, Georgia.

Yu, Y-M, Ma, N, Fan, S-M, and Gu, X-C (2017). "Experimental and numerical studies on sloshing in a membrane-type LNG tank with two floating plates," *Ocean Eng*, 129, 217–227.

Zhang, G, Zhao, W, and Wan, D (2022). "Numerical simulations of sloshing waves in vertically excited square tank by improved MPS method," *J Hydrodyn*, 34(1), 76–84.

Zheng, J, Xue, M-A, Dou, P, and He, Y (2021). "A review on liquid sloshing hydrodynamics," *J Hydrodyn*, 33(6), 1089–1104.

Zheng, X, Li, X, and Ren, Y (2012). "Equivalent mechanical model for lateral liquid sloshing in partially filled tank vehicles," *Math Probl Eng*, 2012, 1–22.

Zhou, Y, Qian, L, and Bai, W (2023). "Sloshing dynamics of a tuned liquid multi-column damper for semi-submersible floating offshore wind turbines," *Ocean Eng*, 269, 113484.